Critical evaluation of approximate quantum decoherence rates for an electronic transition in methanol solution

László Turi[a]

Eötvös Loránd University, Department of Physical Chemistry, Budapest 112, P. O. Box 32, H-1518, Hungary

Peter J. Rossky[b]

Institute for Theoretical Chemistry, Department of Chemistry and Biochemistry, University of Texas at Austin, Austin, TX 78712-1167

We present a quantum molecular dynamics calculation of a semiclassical decoherence function to evaluate the accuracy of alternative short-time approximations for coherence loss in the dynamics of condensed phase electronically non-adiabatic processes. The semiclassical function from mixed quantum-classical molecular dynamics simulations and frozen Gaussian wave packets is computed for the electronic transition of an excited state excess electron to the ground state in liquid methanol. The decoherence function decays on a 10 fs timescale qualitatively similar to the aqueous case. We demonstrate that it is the motion of the hydrogen atom, and in particular, the hydrogen rotation around the oxygen-methyl bond which is predominantly responsible for destroying the quantum correlations between alternative states. Multiple timescales due to the slower diffusive

[a] e-mail: turi@para.chem.elte.hu

[b] e-mail: rossky@mail.utexas.edu

nuclear modes, which dominate the solvation response of methanol, do not contribute to the coherence loss. The choice of the coordinate representation is investigated in detail and concluded to be irrelevant to the decay. Changes in both nuclear momenta and positions on the two alternative potential surfaces are found to contribute to decoherence, the former dominating at short times ($t < 5$ fs), the latter controlling the decay at longer times. Various short-time approximations to the full dynamics for the decoherence function are tested for the first time. The present treatment rigorously develops the short-time description and establishes its range of validity. Whereas the lowest-order short-time approximation proves to be a very good approximation up to about 5 fs, we also find that it bounds the decay of the decoherence function. After 5 fs, the coherence decay in fact becomes faster than the single Gaussian predicted in the lowest-order short-time limit. This decay is well reflected by an enhanced low-order approximation, which is also easily computed from equilibrium classical forces.

I. Introduction

Due to the large density of accessible states, radiationless non-adiabatic (NA) quantum processes are ubiquitous phenomena in condensed phases. Important manifestations include electron and proton transfer reactions, internal conversion, and intramolecular vibrational energy redistribution.[1,2,3] Non-radiative relaxation processes have received considerable scientific attention in the past few years with the development of new theoretical approaches and experimental techniques.

From a practical computational viewpoint, the accurate quantum dynamical treatment of the large number of degrees of freedom in condensed phases is still prohibitive due to the limitations of computational resources. Pragmatically, most approaches treat a small subset of the system quantum mechanically, while the rest, the "bath", is described classically.[4,5,6,7,8,9,10] The separation of the classical and quantal subsets brings about a technical obstacle: the two types of degrees of freedom must evolve self-consistently. Most quantum-classical molecular dynamics (QCMD) methods address the problem by using either one (or both) of the two main approaches to reach self-consistent dynamics: the mean-field method[11] and/or the Preston-Tully surface hopping approach.[12] Beyond the self-consistency problem, another major issue arises when one attempts to correlate the predictions of the QCMD approach to those of exact quantum dynamics. Recently Berne and co-workers reviewed the adequacy of QCMD methods in condensed phase simulations of various radiative and non-radiative processes

by comparing to exact fully quantum mechanical solutions for accessible models. They concluded that such methods should be used with extreme caution.[13,14]

It was realized in a similar context that the neglect of the dynamics of the bath wave functions in NA QCMD simulations can lead to serious errors.[15] The bath wave functions evolving on alternative adiabatic potential surfaces quickly become orthogonal due to the divergence of the (typically nuclear) paths. Associated is a rapid loss of quantum correlations in the subsystem, i.e., decoherence.[16,17,18,19,20,21,22,23] The phenomenon can be conveniently described by the reduced density matrix (ρ) of the quantum subsystem obtained by tracing the density matrix of the full system over the bath coordinates. Since the off-diagonal elements of this subsystem reduced density matrix involve the overlaps between bath wave functions,[24] it is the fast divergence of the alternative paths (through the decreasing overlap integrals) which is responsible for the decay of the off-diagonal terms of the subsystem reduced density matrix and loss of coherence.[23]

Recently, significant progress has been made in understanding the role decoherence plays in realistic electronically NA processes in condensed phases.[15,25,26,27,28] Apparently, QCMD approaches usually fail to treat decoherence correctly.[15,25] A "decoherence function", leading to dissipation in subsystem dynamics, provides the necessary link between the NA QCMD approaches and the fully quantal treatment.[26] For example, the introduction of decoherence can change NA transition rates dramatically, even by orders of magnitude.[15,25] Simulations with a recently developed dissipative QCMD simulation method give a clear illustration of this effect.[10] Decoherence has also been shown to have significant impact on electron transfer reactions potentially

influencing both the rate and the mechanism.[27,28] A connection between the decoherence function and the equilibrium solvation response function, both inherently determined by the sensitivity of bath evolution to the electronic state of the solute, implies strong correlation with solvation dynamics, as well.[29]

In the present paper we wish to accurately evaluate a semiclassical decoherence function $D(t)$ utilizing the Gaussian wave packet approach to full quantum dynamics. [30,31] In particular, we shall use the frozen Gaussian (FG) based method developed by Neria and Nitzan for evaluating NA transition rates.[32] The thermal transition rate between the initial electronic state 1 and the final electronic state 2 is expressed within perturbation theory (Golden Rule) with FG wave packets as

$$k_{1\to 2}^{qm} = \frac{1}{\hbar^2}\left\langle \int_{-\infty}^{\infty} dt V_{12}^{q-c}(t) V_{21}^{q-c}(0) J(t) \right\rangle_T , \qquad (1)$$

where $V_{12}^{q-c}(t)$ is the time-dependent quantum-classical coupling along the classical trajectory propagated on the initial potential surface, and *J(t)* is the complex valued overlap of the two nuclear wave functions evolving on different potential surfaces. Since *J(t)* and the closely related decoherence function *D(t)* connect the quantum and the quantum-classical rate expressions, accurate evaluation of these quantities from MD simulations is of central importance to understand the role of quantum correlations on rate processes. This evaluation is the fundamental issue we address in the present paper.

As a model for NA transitions, we choose the non-radiative relaxation of an excited state localized solvated electron to its ground state. Due to the strong coupling between the solute electronic states and the solvent fluctuations, the solvated electron is a sensitive probe of the NA processes in (at least) two respects. On one hand, the solvated electron may be used to monitor the solvation dynamics following abrupt changes of the

solute electronic distribution (i.e. electronic transitions), *and*, on the other hand, it may test the influence of solvent fluctuations on the mechanism and the rate of the NA relaxation of the solute. To achieve these goals both experimental[33,34,35,36] and theoretical techniques have been developed and applied for the solvated electron in various solvents in the last two decades.[4,6,7,8,9,37,38,39,40] Several papers have examined the specific role of decoherence in the solvated electron system *per se*. [10,15,25,26,27,28,29,41] The present study goes beyond these previous works based primarily on a lowest-order short-time (ST) approximation.[26] As an equally important goal, we evaluate the applicability of this ST approximation for a potentially challenging case. For this purpose, we shift our attention from aqueous systems, which are characterized by very fast and large amplitude inertial solvent response to NA transitions, to a significantly slower and more complex solvent, methanol. In methanol, the solvation response to a change in solvent-solute interaction manifests times from tens of fs to picoseconds.[42,43] At the same time the shortest time inertial dynamics accounts for a rather small part of the response,[40,44] in contrast to water.[38,44] Hence one might well question whether the short time dynamics determined only by the initial positions and forces acting on the nuclei are sufficient to completely determine the coherence decay. While electron solvation in methanol has been investigated in QCMD simulations on several occasions, [39,40,44,45,46,47] the present work focuses on the general understanding of the relation of the physics of solvation processes and those of subsystem coherence loss.

The structure of the paper is as follows. First, we review the FG method, the definition of the decoherence function, the approximations involved in the definition, and, in particular, the short-time approximation for this decoherence function. Choices of

coordinate system representation for the nuclear dynamics and their connection are also discussed. Sec III contains the description of the model (equilibrium first excited state solvated electron in methanol) and the computational details of the simulations. We present and analyze the decoherence dynamics in comparison with its various approximations, emphasizing those which are readily evaluated from equilibrium classical bath quantities. A subsequent discussion on the relation between solvation dynamics and decoherence closes the section. Sec IV concludes the paper.

II. Methods

II.1. The decoherence function in the FG formalism

Following Neria and Nitzan,[32] in the FG approximation, the nuclear wave function $|G_\alpha(t)\rangle$ is approximated by the product of Gaussian wave packets:

$$|G_\alpha(t)\rangle = \prod_n G_{\alpha n}(\mathbf{x},\mathbf{p},t)\exp\left[\frac{i}{\hbar}\int_0^t L_\alpha(\tau)d\tau\right], \quad (2)$$

with

$$G_{\alpha n}(\mathbf{x},\mathbf{p},t) = \left(\frac{a_n}{\pi}\right)^{3/4} \exp\left[-\frac{a_n}{2}\left(\mathbf{x}-\mathbf{x}_{\alpha n}(t)\right)^2 + \frac{i}{\hbar}\mathbf{p}_{\alpha n}(t)\cdot\left(\mathbf{x}-\mathbf{x}_{\alpha n}(t)\right)\right] \quad (3)$$

where $a_n^{-1/2}$ is the (frozen) width of the *n*th nuclear wave packet, while L_α is the Lagrangian. Frozen Gaussians evolve on the adiabatic potential surfaces and follow purely classical dynamics with position $\mathbf{x}_{\alpha n}(t)$ and momentum $\mathbf{p}_{\alpha n}(t)$ for the *n*th nuclear mode. The FG approximation is expected to be valid at short times, that is, as long as the

wave function remains localized.[26,32] Following Refs 26 and 32, the complex valued overlap of the nuclear wave functions on the diverging α=1 and α=2 adiabatic electronic surfaces

$$J(t) = \langle G_2(t) | G_1(t) \rangle \qquad (4)$$

can be evaluated analytically leading to the following expressions:

$$J(t) = J_{overlap}(t) J_{phase}(t), \qquad (5)$$

where

$$J_{phase}(t) = \exp\left[\frac{i}{\hbar} \int_0^t (\Delta E_{12}(\tau) - \Delta K_{12}(\tau)) d\tau \right] \qquad (6)$$

and

$$\begin{aligned} J_{overlap}(t) = \prod_n & \exp\left[-\frac{a_n}{4} (\mathbf{x}_{2n}(t) - \mathbf{x}_{1n}(t))^2 \right] \\ & \times \exp\left[-\frac{1}{4 a_n \hbar^2} (\mathbf{p}_{2n}(t) - \mathbf{p}_{1n}(t))^2 \right] \\ & \times \exp\left[\frac{i}{2\hbar} (\mathbf{x}_{2n}(t) - \mathbf{x}_{1n}(t))(\mathbf{p}_{2n}(t) + \mathbf{p}_{1n}(t)) \right] \end{aligned} \qquad (7)$$

$J_{phase}(t)$ is an oscillatory function containing the potential energy (the electronic energy) difference, and the kinetic energy difference for the nuclear dynamics on the two different potential surfaces, while $J_{overlap}(t)$ is the (real) overlap between individual nuclear wave packets neglecting the overlap cross terms between different nuclei. Note that both nuclear trajectories in Eq (4) (evolving on the final and the initial electronic surfaces) start from the same initial conditions, classical positions and momenta sampled from the initial potential surface.

With the specific FG functional form for the nuclear wave function and a decorrelation assumption the Golden Rule formula for the NA transition rate (see Eq (1)) can be expressed as[26]

$$k_{1\to 2}^{qm} = \frac{1}{\hbar^2}\int_{-\infty}^{\infty} dt \left\langle V_{12}^{q-c}(t) V_{21}^{q-c}(0) \exp\left[\frac{i}{\hbar}\int_0^t \Delta E_{12}(\tau) d\tau\right]\right\rangle_T \left\langle D(t)\right\rangle_T . \qquad (8)$$

The decoherence function $D(t)$ is defined as

$$D(t) = \exp\left[-\frac{i}{\hbar}\int_0^t \Delta K_{12}(\tau) d\tau\right] J_{overlap}(t). \qquad (9)$$

Eqs (8) and (9) clearly indicate that, within perturbation theory for the NA transition rates, the decoherence function represents the correction between the quantum-classical and the quantum formulas in the frozen Gaussian wave packet approximation. We note a slight difference in the definition relative to Ref 26: in the phase terms of Eqs (8) and (9), we use the rigorous integration of the potential energy and the kinetic energy. This frozen Gaussian/classical dynamics-based form for the decoherence in Eq (9) is a well-defined semiclassical approximation which neglects contributions from wave packet spreading and non-classical paths, and, in particular, does not explicitly treat interference between amplitudes on alternative potential surfaces. The assumption underlying this approximation is that coherence will be lost in condensed phases before such effects become important. It is also important to point out that *D(t)* can be considered as a sensitive measure of decoherence. Due to the connection of $D(t)$ and $J_{\text{overlap}}(t)$ (Eq (9)), and the fact that the off-diagonal elements of the electronic reduced density matrix involve the overlap between bath wave functions, the decay of *D(t)* directly reflects the decay of the coherences in that matrix. Although conventionally other measures of decoherence are often used (for example, the exponent of the "fringe visibility function",

the linear entropy, or Tr[ρ^2]),[17] the use of *D(t)* is especially appealing within the QCMD methodology due to its explicit role as a correction factor relating the quantum-classical and the quantum rate formulas.

As just noted, Tr[ρ^2] has been introduced as a measure of decoherence[19,20] or, more precisely, as a measure of the purity of a quantum state, and we comment briefly here on this alternative before proceeding. The advantage of the measure Tr[ρ^2] is that it is invariant with respect to a change of basis. Creation of a diagonal reduced density matrix alone can always be done in some basis at any instant in time, even if the quantum states retain coherence. However, in the preferred (pointer) basis, the density matrix will evolve to a diagonal form due to coherence loss, and, in this case, the associated decay of the off-diagonal elements is sufficient to characterize the process.[21] The preferred states are the energy eigenstates when the environment is adiabatic.[22] Hence, the dynamical decay of the off-diagonal elements is routinely used in the literature as a means to characterize decoherence.[21,22,23] In fact, the recent development in Ref 23 closely parallels that in the earlier work of Prezhdo and Rossky[26] and that summarized here in Eq (21). It is perhaps worth noting that in the present context, where the quantum electronic system decays, in effect irreversibly, from the pure excited state to what is essentially the pure ground state, Tr[ρ^2] would, in fact, be expected to decrease initially, but then increase again as ground state equilibrium is established. The latter population dynamics, of course, has no immediate relationship to coherence evolution.

Application of the first-order cumulant expansion for the ensemble average of the decoherence function and the lowest-order short-time approximation (ST) for the power series of $\mathbf{x}_{\alpha n}(t)$ and $\mathbf{p}_{\alpha n}(t)$ of $J_{overlap}(t)$ leads to a particularly useful expression:[26]

$$\langle D(t)\rangle_T \approx \langle J_{overlap}(t)\rangle_T \approx \exp\left[-\left\langle \sum_n \frac{1}{4a_n\hbar^2}(\mathbf{F}_{1n}(0)-\mathbf{F}_{2n}(0))^2 \right\rangle_T t^2\right] \quad (10)$$

According to Eq (10) the decay of the decoherence function can be approximated as a single Gaussian function with a characteristic decoherence time

$$\tau_D = \left[\left\langle \sum_n -\frac{1}{2a_n\hbar^2}(\mathbf{F}_{1n}(0)-\mathbf{F}_{2n}(0))^2 \right\rangle_T\right]^{-1/2}. \quad (11)$$

The numerical evaluation of the ST decoherence function from real time MD simulation requires only the equilibrium trajectory of the system on the initial surface. Since frozen Gaussians evolve along the classical trajectory, it is sufficient to describe the nuclear propagation by classical dynamics. One can then simply calculate the force difference upon the classical bath from the quantum subsystem in the initial and the final states along this trajectory.

The fully dynamical evaluation of Eq (9) requires more elaborate calculations. Although an equilibrium initial state trajectory is still needed, it is only a starting point of the procedure. The decoherence function $D(t)$ is computed from the parallel evolution of the two diverging nuclear wave functions on the initial and the final surfaces starting from the same initial classical positions and momenta.[32] The initial conditions are sampled from the adiabatic equilibrium trajectory of the initial surface to achieve thermal averaging.

Due to the classical nature of the nuclear evolution, the only unknown parameter of the FG approach is the width of the wave packets of the individual nuclear modes $a_n^{-1/2}$. Neria and Nitzan derived the exact analytical expression for the width of the FG

wave packets within the displaced harmonic oscillator model.[32] The analytical expression contains the reduced mass m_n and eigenfrequency ω_n of the n-th nuclear mode:

$$a_n = \frac{m_n \omega_n}{\hbar} A_n \qquad (12)$$

where

$$A_n = \left[\coth\left(\frac{\hbar \omega_j}{2k_B T} \right) - \frac{2k_B T}{\hbar \omega_j} \right]^{-1} \qquad (13)$$

The same width can be obtained from the variational effective harmonic treatment of Feynman and Kleinert,[48] for highly localized nuclear wave packets. In the high temperature limit Eq (12) takes a simpler form which is independent of the frequency of the nuclear modes.

$$a_n = \frac{6 m_n k_B T}{\hbar^2} \qquad (14)$$

Below we shall use both definitions of a_n, and assess their effect on the decoherence function. The assignment of nuclear mode frequencies in the analytical harmonic expression (Eqs (12) and (13)) is also a delicate issue which can be addressed only in conjunction with the proper choice of coordinate system. Although the instantaneous normal mode (INM) treatment of the solvated electron system has been developed successfully,[49] for the present work we use the simpler atomistic Cartesian coordinate system (CC, only applicable in the high temperature limit) and a single molecule-based normal coordinate system (quasi normal modes, QNM) similar in philosophy to that of Prezhdo and Rossky.[50] The computational details of QNMs and the assignment of the frequencies are given in the next section. We will demonstrate below that the

decoherence function is insensitive to the choice of coordinate system for our model. Thus, the simpler CC and QNM treatments are sufficient.

II.2. Coordinate systems: Cartesian coordinates and quasi normal modes

The evolution of the nuclear subsystem is described in terms of two different coordinate systems, atomic Cartesian coordinates and single molecule quasi normal modes. The simulations are performed in Cartesian coordinates and orthogonal transformations to QNMs are performed at each time step. In the QNM approach, every molecule is treated individually, neglecting its interaction with the environment. The transformation of Cartesian vectors (displacement, momentum and quantum force in Eqs (7) and (10)) is performed in the mass-weighted Cartesian coordinate system and is based on the projection of the vectors onto the basis vectors of the individual molecular modes. As usual, three modes correspond to the center-of-mass motion (translation) and three to rotations around the instantaneous principal axes. The basis vectors for the remaining three modes, the intramolecular vibrations, are constructed from the normal modes of the isolated methanol molecule at its equilibrium configuration. The exact normal modes, starting with the OH stretching normal mode, the COH bending and the CO stretching mode, are then orthogonalized by successive application of the Gram-Schmidt orthogonalization procedure to the six instantaneous basis vectors of the translational and rotational motions for each molecule in the simulation box. The nine basis vectors form the transformation matrix which projects out the individual components of the Cartesian vectors. We note that the transformation matrix, and the procedure employed here, is the

analog of that used in large-scale ab initio quantum chemistry. Thus, at every time step a new orthogonal transformation is performed to transform the Cartesian vectors to QNMs. Clearly, the QNM analysis is not fully rigorous in the sense that QNMs are not eigenvectors of the Hessian, and they slightly change during the time evolution of the system. Nevertheless, the QNM treatment allows one to decompose the complicated multi-body dynamics of the system to (approximate) individual molecular motions with well-defined physical interpretation. In contrast, the otherwise rigorous INM analysis is hampered by the appearance of imaginary frequency modes.[41,49] The development of the QNM analysis also reveals that within the high-temperature approximation for the Gaussians, the three coordinate systems should predict an identical decoherence function in the ST limit (Eq (10)) and nearly identical functions in the exact treatment (Eq. (9)).

To illustrate the point let us insert Eq (14) to Eq (10) in Cartesian coordinates leading to

$$\langle D(t)\rangle_T = \exp\left[-\frac{1}{24k_BT}\left\langle \sum_n \left(\frac{\mathbf{F}_{1n}(0)-\mathbf{F}_{2n}(0)}{\sqrt{m_n}}\right)^2 \right\rangle_T t^2\right]. \qquad (15)$$

The expression within the bracket is the square of the total force in the $3N$-dimensional mass-weighted Cartesian coordinate system, where N is the number of atoms (N = 600 in our simulations). Since, orthogonal transformations do not change this quantity, the ST decoherence function in the high-temperature limit remains unaffected upon either QNM or INM transformations, for example. Similar argument proves that the exponent of the first exponential of $J_{\text{overlap}}(t)$ in Eq (7) would also be independent of the choice of the coordinate system in the high-temperature limit. While the second and third terms change upon transformation (due to the different reference geometries), we illustrate in the next

section that for practical purposes this effect is negligible. In addition, the exact analytical expression of Eq (12) contains the frequencies of the nuclear modes which exclude the possibility of similar simplification. Below, we shall also examine the effects of transformations and temperature dependence of the width of the Gaussians on the decoherence function.

For the assignment of frequencies to quasi normal modes, we take the experimental IR vibrational frequencies of liquid methanol,[51] and use them as average frequencies in the analysis. This approach has been successfully applied for the aqueous case.[26] The frequency of the OH stretch is 3337 cm^{-1}, 1429 cm^{-1} for the COH bend, and 1029 cm^{-1} for the CO stretch. Experimentally, only one broad band is observed in the librational regime at 655 cm^{-1}. Since this peak shifts by $\sqrt{2}$ to lower frequencies upon deuteration to CH_3OD, we assign this peak to the hindered rotation around the *x*-axis (essentially around the O-Me bond). Assuming the same force constants for the other two rotations, around the axis perpendicular to the *x*-axis in the molecular plane of the three-site model (*z*-axis) and around the axis perpendicular to the molecular plane (*y*-axis), and using the moments of inertia values calculated from the normal mode analysis of the methanol molecule at its equilibrium configuration, we estimate the librational frequencies for the *y* and *z*-rotations to be 260 cm^{-1} and 240 cm^{-1}, respectively. For translational motions we set the frequency to 100 cm^{-1}, a choice which is not consequential here as long as the value is in the low frequency regime.

III. Results and Discussion

We performed mixed quantum classical simulations of an excited state solvated electron in a methanol bath in the NVE ensemble. The simulation details are similar to those in Ref. 39. The bath consists of 200 methanol molecules in a cubic simulation cell described by a three-site classical potential and internal flexibility. Although there exists some indication that the methyl hydrogens of the methanol molecules can weakly interact with the localized electron,[52] based on our previous simulations[39,40] we expect, that the present three-site model is suitable to capture the major aspects of the investigated physical problem. The electron is treated quantum mechanically in a plane wave basis represented on 32^3 evenly spaced gridpoints in the simulation box.[37] The interaction between the quantum particle and the classical molecules is modeled by the modified pseudopotential of Zhu and Cukier.[39,53] The nuclear configurations are adiabatically propagated on the potential surfaces using the sum of classical and Hellman-Feynman forces. The simulation time step is 1 fs. The long-range part of the interactions and the forces are calculated here using the Ewald summation technique including solvent-solvent and the solvent-electron interactions explicitly.[54]

First, we generated a 40 ps long equilibrium excited state trajectory of an excess electron in a methanol bath. The system temperature averages 298 K. The eigenenergy of the first (occupied) excited state is −0.388 eV. All other higher energy excited states are unbound in the sense that they have positive eigenenergies. The average energy gap between the first excited state and the unoccupied ground state is 0.253 eV with 0.113 eV standard deviation. Although previous calculations on the ground state solvated electron in methanol were performed with a smooth spherical cutoff for the long-range interactions, [39,40,44,45,46,47] the present numbers are consistent with those data. The initial

conditions (classical positions and momenta) for the calculation of the nuclear overlap and the decoherence function are sampled from the equilibrium excited state trajectory at every 2 ps for the total of 20 configurations. Starting from the selected configurations and velocities of the excited state, we simulated 20 adiabatic trajectories of 200 fs length evolving on the final (ground) electronic state. The corresponding excited state nuclear evolutions were taken from the equilibrium trajectory starting from the same initial conditions.

Now we turn our attention to the calculation of the decoherence function. At the outset, we examine the semiclassical decoherence function within the FG approximation as defined in Eqs (7) and (9), and first evaluate the effect of the coordinate system transformations and of the width of the frozen Gaussians on the computed quantities. Then various approximations will be tested, in particular, the first-order cumulant expansion of the ensemble average of the decoherence function and the short-time approximation of $J_{\mathrm{overlap}}(t)$, and compared to the full semiclassical decoherence function. An important element is a discussion on the relationship between solvation dynamics and decoherence function in terms of various nuclear contributions to the solvent relaxation.

Figure 1 presents the real part of the ensemble average of the decoherence function in quasi normal mode representation using both the exact T-dependent expression (Eqs (12) and (13)) (QNM/ET) and the high-temperature limit (Eq (14)) (QNM/HT) for the width of the Gaussians at 298 K. For comparison, we also show the HT result in Cartesian coordinates (CC/HT). First, one notices that the QNM/HT and CC/HT functions differ only insignificantly, indicating that for the present system the orthogonal coordinate transformation has only negligible effect on the decoherence

function. Based on this observation, one expects a very similar function in INMs, as well. Second, it is also clear from the essentially indistinguishable QNM/ET and QNM/HT functions that for the present case the high-temperature approximation is a viable one. Since the HT approximation at room temperature is not suitable for the highest-frequency modes,[41] one can already anticipate that the mechanism for the coherence loss is not dominated by these highest-frequency nuclear motions. Nevertheless, for the sake of consistency and rigor, we shall use QNMs and the exact *T*-dependence of the Gaussian widths in the remainder of the paper.

The inset to Fig 1 also shows the real part of the decoherence function for 20 individual trajectories. It is interesting to note how different the timescale of the relaxation is for the different trajectories, and how efficiently the averaging process leads to a smooth result. The ensemble average of the decoherence function decays very quickly losing half of its amplitude by around 10 fs, effectively reaching zero by 30 fs. The decay rate is somewhat slower, but qualitatively similar to that found for the hydrated electron in the short-time approximation[26] and using INM dynamics.[41] An interesting feature appears in the decoherence function at ~20 fs, as a distinct recurrence is observed. We believe that the recurrence is not likely attributable to statistical noise; performing the calculation for each of two 10 trajectory subsets, the recurrence appears essentially at the same position. In addition, the ensemble average of the imaginary part of the calculated *D(t)* is negligible in magnitude relative to the real part. Thus, the modulus of the calculated decoherence function is basically identical to the function shown in Fig 1. We will return to this recurrence in a little more detail below.

In the following steps we set out to examine the effects of various approximations to the dynamical FG treatment of the decoherence function. First, we consider decorrelation of the two terms of the decoherence function,[26]

$$\left\langle D(t)\right\rangle_T = \left\langle \exp\left[-\frac{i}{\hbar}\int_0^t \Delta K_{12}(\tau)d\tau\right] J_{overlap}(t)\right\rangle_T \approx \left\langle \exp\left[-\frac{i}{\hbar}\int_0^t \Delta K_{12}(\tau)d\tau\right]\right\rangle_T \left\langle J_{overlap}(t)\right\rangle_T . \tag{16}$$

Using the cumulant expansion to the first order, we then obtain

$$\left\langle D(t)\right\rangle_T \approx \exp\left[-\frac{i}{\hbar}\int_0^t \left\langle \Delta K_{12}(\tau)\right\rangle_T d\tau\right]\left\langle J_{overlap}(t)\right\rangle_T . \tag{17}$$

Since the mean kinetic energy difference vanishes to the second order in time, a reasonable approximation is[26]

$$\left\langle D(t)\right\rangle_T \approx \left\langle J_{overlap}(t)\right\rangle_T . \tag{18}$$

We refer to Eq (18) as the overlap approximation.

Figure 2 illustrates that the approximations involved in Eqs (16)-(18) produce satisfactory agreement with the full decoherence function. It should be pointed out that it is the decorrelation assumption of Eq (16) which leads to the disappearance of the recurrence at ~20 fs, indicating that some correlation exists between the kinetic energy and the overlap function. This is not surprising due to the nuclear velocity dependence of the wave packet position. Nevertheless, the real part of the decorrelated decoherence function fits well to the reference function. Although the agreement of Eq (18) with the full calculation is slightly degraded below 20 fs, it is notable that a remnant of the recurrence appears here.

Since $J_{\text{overlap}}(t)$ is a product of exponential functions (see Eq (7)), application of the first-order cumulant expansion to Eq (18) is a straightforward route for further simplifications:

$$\begin{aligned}\langle D(t)\rangle_T &\approx \exp\langle \ln J_{overlap}(t)\rangle_T \\ &= \exp\left[-\left\langle \sum_n \frac{a_n}{4}\left(\mathbf{x}_{2n}(t)-\mathbf{x}_{1n}(t)\right)^2\right\rangle_T\right] \\ &\times \exp\left[-\left\langle \sum_n \frac{1}{4a_n\hbar^2}\left(\mathbf{p}_{2n}(t)-\mathbf{p}_{1n}(t)\right)^2\right\rangle_T\right] \\ &\times \exp\left[\frac{i}{2\hbar}\left\langle \sum_n \left(\mathbf{x}_{2n}(t)-\mathbf{x}_{1n}(t)\right)\left(\mathbf{p}_{2n}(t)+\mathbf{p}_{1n}(t)\right)\right\rangle_T\right] \\ &\equiv \langle D_x(t)\rangle_T \times \langle D_p(t)\rangle_T \times \langle D_{xp}(t)\rangle_T\end{aligned} \tag{19}$$

Eq (19) breaks the decoherence function into three separate contributions, the first depending on the positions, the second on the momenta and the third, an oscillatory phase term involving both. The real part of $\langle D(t)\rangle_T$ from Eq (19) is shown in Figure 3, with separate contributions from the positions, the momenta and the real part of the oscillatory cross term. Once again, the approximated decoherence function reproduces the full one quite well. At this point, however, we are able to gain additional insight into the role of the individual components of Eq (19). Evidently, the first term depending on the displacements between the nuclear coordinates on two surfaces at the same time plays the dominant role in the loss of the phase information between diverging nuclear paths. The momentum difference on the two electronic surfaces, the second term, contributes to a lesser but not insignificant extent. We note at the outset that the relatively slow decay of $\langle D_p(t)\rangle_T$ evident in the figure for times greater than 15 fs may be due to the small available sample of twenty trajectories. However, this decay plays only a minor role in

the overall decay of $D(t)$. The oscillatory part varies particularly slowly, especially in the first 20 fs, hardly influencing the product in the most critical time window. Using a power series expansion in time of the imaginary exponent, one finds that the exponent vanishes through second order. Further, one finds similar higher order terms and behavior as that for $J_{\text{phase}}(t)$, justifying the neglect of the position-momentum cross term. The product of the remaining two real valued Gaussians provides an excellent description of the full function. Additionally, this simple analytical product form is well suited for further analysis.

In fact, we are now in the position to interpret the decoherence function in terms of the underlying microscopic details, the separate molecular modes. To address the problem, we sum the contributions of the individual molecular modes for all the molecules of the bath:

$$\begin{aligned}\left\langle D(t)\right\rangle_T &\approx \left\langle D_x(t)\right\rangle_T \times \left\langle D_p(t)\right\rangle_T \\ &= \exp\left[-\sum_i \left\langle \sum_m \frac{a_i}{4}\left(\mathbf{x}_{2m}^{(i)}(t)-\mathbf{x}_{1m}^{(i)}(t)\right)^2 \right\rangle_T\right] \\ &\times \exp\left[-\sum_i \left\langle \sum_m \frac{1}{4a_i\hbar^2}\left(\mathbf{p}_{2m}^{(i)}(t)-\mathbf{p}_{1m}^{(i)}(t)\right)^2 \right\rangle_T\right] \\ &\equiv \exp\left[-\sum_i \left\langle d_{i,x}(t)\right\rangle_T\right] \times \exp\left[-\sum_i \left\langle d_{i,p}(t)\right\rangle_T\right]\end{aligned} \tag{20}$$

In Eq (20), the index i stands for the summation over the molecular modes, while m runs over the individual molecules. The exponents $d_{i,x}(t)$ and $d_{i,p}(t)$ are time-dependent displacement and the momentum contributions of the i-th molecular mode to the decoherence function. It is important to note that similarly to previous observation on the long range character of the coherence loss contributions,[28,45] we find here that practically

all 200 molecules in our system contribute to decoherence. Therefore, it is necessary to perform the summation in Eq (20) for all molecules in the simulation box.

The time evolution of the exponents of the separate contributions, shown in Figures 4 and 5, is revealing in many respects. Since, the nuclear modes with larger contributions to the exponents contribute more strongly to the loss of coherence, the contributions from molecular displacements are evidently overall more important than those due to the change of nuclear momentum, despite the fact that $D_p(t)$ contributes at lower order in a short time expansion. If one expands both exponents of Eq (20), one finds that that the dominating contributions of the exponent are provided through order t^4, and are given by the lowest-order non-vanishing terms for each exponent:

$$\langle D(t)\rangle_T \approx \exp\left[-\left\langle \sum_n \frac{a_n}{16m_n^2}\left(\mathbf{F}_{1n}(0)-\mathbf{F}_{2n}(0)\right)^2\right\rangle_T t^4\right]\times\exp\left[-\left\langle \sum_n \frac{1}{4a_n\hbar^2}\left(\mathbf{F}_{1n}(0)-\mathbf{F}_{2n}(0)\right)^2\right\rangle_T t^2\right]. \tag{21}$$

The most distinctive feature of Fig 4 is the striking extent to which the displacement of the hydrogen rotational mode around the O-Me bond determines decoherence. By around 20 fs the weight of the contribution from the hydrogen rotation exceeds all other modes at least by an order of magnitude. The next two most significant contributions are also due to the differing motions of the hydrogen on the diverging potential surfaces through the COH bend and the OH stretch. After approximately 20 fs, essentially all displacement contributions become sizable, but this change does not influence the decoherence function significantly, since it already approaches zero by this time. Fig 4 also indicates that the relative weight of the individual contributions change in time. This effect is especially interesting at the very early stage of the dynamics, under 5 fs as shown in Fig 5. Although the major component of the coherence loss still originates

from the hydrogen motions (*x*-rotation and COH bend), it is now the change of the momentum which plays the most important part in the mechanism. It is only after 5 fs that contributions from the displacement change gradually dominate. Fig 5 demonstrates that at very short times, $t \leq 5$ fs, mainly the t^2 term of Eq (21) ($\langle D_p(t) \rangle_T$) determines the decoherence function. Correspondingly, this is the time regime where the decoherence function can be well approximated by the ST approximation of Eq (10). For longer times, as the displacement term (starting with the t^4 term in the time expansion, as in Eq (21)) starts dominating, one can expect even faster coherence loss than can be anticipated from the t^2 term alone.

Figure 6 lets us examine how the ST approximation fares at longer times relative to the full calculation. Interestingly, while the ST function employing the exact *T*-dependence for the width of the wave packets predicts somewhat slower relaxation (τ_D = 12.6 fs), the high-temperature limit reproduces the exact behavior quite well (τ_D = 9.9 fs). This agreement is necessarily fortuitous. The role of the molecular mode contributions can be easily visualized in the ST-limit with the summed coefficients of the t^2 term, d_i, for the individual modes in Eqs (10) and (21).[26] Such separation for analysis is supported by the discussion above. The static picture of Figure 7, corresponding to the very early times of the dynamics, conveys similar qualitative information as Figures 4 and 5, indicative of the dominance of the OH rotation. Overall, the ST approximation provides a reasonable framework to study the decoherence function, being basically equivalent at short times and giving a reasonable approximation to the full function at longer times. Nevertheless, the performance of the ST expression can be very easily improved in principle by adding the t^4 term as in Eq (21), requiring no additional information. The resulting t^4-corrected

ST function now shows faster decay than the full function in Fig 6, indicating that inclusion of other higher order terms would be necessary to achieve an even more precise description. To quantify the decoherence rate for the functions in Fig 6, we can employ the conventional definition of a characteristic time as the integral of the function, $\tau_d = \int_0^\infty D(t)dt$. According to this definition, the coherence dissipation time is τ_d = 12 fs for the full semiclassical function, compared to τ_d = 16 fs or τ_d = 13 fs for the lowest-order short-time approximation with either the exact model temperature dependence or in the high-temperature limit, respectively. The t^4-corrected ST function yields a coherence dissipation time of τ_d = 8 fs.

Now we examine the possible implications of decoherence for the solvation dynamics. Prezhdo and Rossky developed a quantitative relationship between short-time quantum coherence loss and short-time solvent response, and illustrated the connection between the two phenomena for the case of electron hydration.[29] Water, however, is the fastest solvent, giving enormous short-time response.[38] The question, thus, arises: what happens in an apparently very different solvent, such as methanol, which manifests multiple timescales which are both significantly slower and carry greater amplitude than the inertial component of the solvation response. Figure 8 demonstrates this behavior for both the non-equilibrium solvent response $S(t)$ following the electronic relaxation from the excited state to the ground state as calculated from non-equilibrium average of the electronic energy gap for the 20 trajectories

$$S(t) = \frac{\overline{\Delta E}(t) - \overline{\Delta E}(\infty)}{\overline{\Delta E}(0) - \overline{\Delta E}(\infty)}, \qquad (22)$$

and its approximation in the linear response regime $C(t)$ calculated from the fluctuations of the equilibrium energy gap

$$C(t) = \frac{\langle \delta\Delta E(0)\delta\Delta E(t)\rangle}{\langle \delta\Delta E^2\rangle} \quad . \qquad (23)$$

We note that for the asymptotic energy gap in Eq (22) we used 1.5 eV, the value from our previous simulation without explicit treatment of long-range interactions.[39] It is evident from Figure 8 and from the solvation dynamics analysis of Ref. 44 that the inertial component of the solvation dynamics plays only a minor role in the solvation response. The non-equilibrium and the equilibrium response functions deviate from each other significantly in the computed 200 fs range. This case, thus, provides another example for the breakdown of the linear response approximation in methanol.[42,47] A fit of a Gaussian and two exponentials to $C(t)$ indicates a rather fast inertial component with τ_g = 4 fs characteristic time but only ~5% contribution to the full relaxation amplitude. The two slower exponentials relax on the 0.1 and 1.5 ps timescale similar to those found in a previous analysis.[44] The estimate for the inertial time scale based on the quantitative relationship between ST decoherence and solvation dynamics,[29] τ_g = 14 fs, is in a better agreement with the inertial part of $S(t)$.[12] The non-equilibrium response relaxes on two timescales, a 12 fs Gaussian contributes 20 % to the relaxation, while the rest is fitted by a single exponential decay of 500 fs characteristic time within the available 200 fs window. As pointed out previously,[44] the inertial component of the relaxation is mainly due to the hydrogen rotation around the C-O bond, but it is the longer timescale diffusive motions that are responsible for the overwhelming majority of the solvation response. The same nuclear mode, hydrogen rotation destroys coherence in the nuclear wave

function more effectively within 20-25 fs, because the coherence loss is described by a product over modes, while decay of the energy has roughly additive components. By the time the slower diffusive components would become important in the coherence loss, the nuclear trajectories have already lost correlation.

IV. Conclusions

In the present work we have performed a real time quantum molecular dynamics analysis of the decoherence function for the electronic relaxation of an excited state solvated electron to its ground state in methanol. The analysis is based on the application of mixed quantum-classical molecular dynamics trajectories and the frozen Gaussian approximation formalism for the nuclear wave function developed originally by Neria and Nitzan.[32] We applied Cartesian coordinates as well as single molecule based quasi normal modes in the analysis and pointed out that the choice of the coordinate system does not bear any real significance on the decoherence function as long as the coordinates are derived from mass-weighted Cartesians by an orthogonal transformation.

The computed semiclassical decoherence function shows an ultrafast decay on the 10 fs time scale, thereby providing an *a posteriori* justification for the use of the FG approximation. Although this decay is somewhat slower than in water, the similarity of the time scales is striking. In particular, we find, that the multiple diffusive timescales characteristic of the solvation processes in methanol do not significantly influence the decay of the decoherence function. We have demonstrated that the loss of coherence is almost exclusively dominated by the hydrogen rotation around the methyl-oxygen bond,

the same mode which controls the inertial part of the solvation dynamics. The faster decoherence in water can be attributed to the fact, that while there exist three rotational degrees of freedom for rotation in water with low moments of inertia, there is only one such rotation in methanol as analyzed previously in the context of solvation dynamics.[44] Detailed investigation into the role of the molecular modes reveals that both the change of the momentum and the change of the position of the nuclear modes on the ground electronic surface relative to the excited state influence the decoherence function. The relative weight of the individual contributions to decoherence is time-dependent. At the shortest times (< 5 fs) the momentum difference dominates, at longer times (5 fs < t < 25 fs) the displacement of the mode coordinates determines the coherence loss. Contributions of the diffusive motions, which are responsible for the majority of solvation response in methanol, become significant only after the coherences are already effectively destroyed. One can then conclude that although both coherence loss and solvation dynamics are determined by bath evolutions, their sensitivity to individual bath nuclear modes can be quite different. While, the OH inertial rotation is the major factor for decoherence, it plays only a relatively minor role in the total solvation dynamics in methanol.

The effects of various approximations on the decoherence function have also been tested. In particular, we established a rigorous background for the short-time approximation and examined its applicability. We found that the lowest-order ST approximation provides a reasonable framework to study the decoherence function. The ST decoherence function performs excellently at short times, and gives a reasonable approximation of the full semiclassical function at longer times.

Acknowledgment

L.T. gratefully acknowledges the tenures of the Eötvös Fellowship, the Bolyai Research Fellowship, and the hospitality of the Institute for Theoretical Chemistry, University of Texas at Austin. The work was supported by grants to L. T. from the Foundation for Hungarian Higher Education and Research, Ministry of Education, Hungary (research grant No. 0140/2001) and from the National Research Fund of Hungary (OTKA) under Contract No. F031996.

This work was also supported by a grant to P. J. R. from the National Science Foundation (CHE-0134775) and by the R. A. Welch Foundation.

References

[1] J. Jortner and M. Bixon, Editors, "Electron Transfer - from Isolated Molecules to Biomolecules" in *Advances in Chemical Physics*, Vol. 106-107 (Wiley, New York, 1999).

[2] B. Bagchi and V. Krishnan, Editors, *Solvation Dynamics and Charge Transfer Reactions* (World Scientific Publishing Co., Singapore, 1992).

[3] J. Klafter, J. Jortner, and A. Blumen, Editors, *Dynamical Processes in Condensed Molecular Systems* (World Scientific Publishing Co., Singapore, 1989).

[4] D. Thirumalai, E. J. Bruskin, and B. J. Berne, J. Chem. Phys. **83**, 230 (1985).

[5] R. Car and M. Parrinello, Phys. Rev. Lett. **55**, 2471 (1985).

[6] M. Sprik and M. L. Klein, J. Chem. Phys. **89**, 1592 (1988).

[7] A. Staib and D. Borgis, J. Chem. Phys. **103**, 2642 (1995).

[8] F. A. Webster, P. J. Rossky, and R. A. Friesner, Comp. Phys. Comm. **63**, 494 (1991).

[9] K. F. Wong and P. J. Rossky, J. Chem. Phys. **116**, 8418 (2002).

[10] K. F. Wong and P. J. Rossky, J. Chem. Phys. **116**, 8429 (2002).

[11] P. Ehrenfest, Z. Phys. **45**, 455 (1927).

[12] R. K. Preston and J. C. Tully, J. Chem. Phys. **55**, 562 (1971).

[13] S. A. Egorov, E. Rabani, and B. J. Berne, J. Chem. Phys. **110**, 5238 (1999).

[14] S. A. Egorov, E. Rabani, and B. J. Berne, J. Phys. Chem. **103**, 10978 (1999).

[15] E. R. Bittner and P. J. Rossky, J. Chem. Phys. **103**, 8130 (1995).

[16] H. D. Zeh, Phys. Lett. A. **172**, 189 (1993).

[17] W. H. Zurek, Prog. Theor. Phys. **89**, 281 (1993).

[18] W. H. Zurek, Rev. Mod. Phys. **75**, 715 (2003).

[19] J. P. Paz, S. Habib, and W. H. Zurek, Phys. Rev. D **47**, 488 (1993).

[20] W. H. Zurek, S. Habib and J. P. Paz, Phys. Rev. Lett. **70**, 1187 (1993).

[21] W. H. Zurek, Nature, **412**, 712 (2001).

[22] J. P. Paz, and W. H. Zurek, Phys. Rev. Lett. **82**, 5181 (1999).

[23] C. P. Sun, X. F. Liu, D. L. Zhou, and S. X. Yu, Phys. Rev. A **63**, 012111, (2001).

[24] M. Simonius, Phys. Rev. Lett. **40**, 980 (1978).

[25] B. J. Schwartz, E. R. Bittner, O. V. Prezhdo, and P. J. Rossky, J. Chem. Phys. **104**, 5942 (1996).

[26] O. V. Prezhdo and P. J. Rossky, J. Chem. Phys. **107**, 5863 (1997).

[27] D. M. Lockwood, H. Hwang, and P. J. Rossky, Chem. Phys. **268**, 285 (2001).

[28] D. M. Lockwood, Y.-K. Cheng, and P. J. Rossky, Chem. Phys. Lett. **345**, 159 (2001).

[29] O. V. Prezhdo and P. J. Rossky, Phys. Rev. Lett. **81**, 5294 (1998).

[30] E. J. Heller., J. Chem. Phys. **68**, 2066 (1978).

[31] E. J. Heller, J. Chem. Phys. **75**, 2923 (1981).

[32] E. Neria and A. Nitzan, J. Chem. Phys. **99**, 1109 (1993).

[33] A. Migus, Y. Gauduel, J. L. Martin, and A. Antonetti, Phys. Rev. Lett. **58**, 1559 (1987).

[34] C. Silva, P. K. Walhout, K. Yokoyama, and P. F. Barbara, Phys. Rev. Lett. **80**, 1086 (1998).

[35] X. Shi, F. H. Long, H. Lu, and K. B. Eisenthal, J. Phys. Chem. **99**, 6917 (1995).

[36] P. K. Walhout, J. C. Alfano, Y. Kimura, C. Silva, P. Reid, and P. F. Barbara, Chem. Phys. Lett. **232**, 135 (1995).

[37] J. Schnitker, K. Motakabbir, P. J. Rossky, and R. Friesner, Phys. Rev. Lett. **60**, 456 (1988).

[38] B. J. Schwartz and P. J. Rossky, J. Chem. Phys. **101**, 6902 (1994).

[39] L. Turi, A. Mosyak, and P. J. Rossky, J. Chem. Phys. **107**, 1970 (1997).

[40] P. Mináry, L. Turi, and P. J. Rossky, J. Chem. Phys. **110**, 10953 (1999).

[41] C.-Y. Yang and P. J. Rossky, submitted for publication.

[42] T. Fonseca and B. M. Ladanyi, J. Phys. Chem. **95**, 2116 (1991)

[43] S. G. Rosenthal, R. Jimenez, G. R. Fleming, P. V. Kumar, and M. Maroncelli, J. Mol. Liq. **60**, 25 (1994).

[44] A. Mosyak, O. V. Prezhdo, and P. J. Rossky, J. Chem. Phys. **109**, 6390 (1998).

[45] A. Mosyak, O. V. Prezhdo, and P. J. Rossky, J. Mol. Struct. **485-486**, 545 (1999).

[46] A. Mosyak, P. J. Rossky, and L. Turi, Chem. Phys. Lett. **282**, 239 (1998).

[47] L. Turi, P. Mináry, and P. J. Rossky, Chem. Phys. Lett. **316**, 456 (2000).

[48] R. P. Feynman and H. Kleinert, Phys. Rev. A **34**, 5080 (1986).

[49] C.-Y. Yang, K. F. Wong, M. S. Skaf, and P. J. Rossky, J. Chem. Phys. **114**, 3598 (2001).

[50] O. V. Prezhdo and P. J. Rossky, J. Phys. Chem. **100**, 17094 (1996).

[51] M. Falk and E. Walley, J. Chem. Phys. **34**, 1555 (1961).

[52] L. Turi, J. Chem. Phys. **110**, 10364 (1999).

[53] J. Zhu and R. I. Cukier, J. Chem. Phys. **98**, 5679 (1993).

[54] M. P. Allen and D. J. Tildesley, *Computer Simulation of Liquids* (Clarendon, Oxford, 1987).

Figure Captions

Figure 1. The real part of the semiclassical decoherence function calculated in QNMs with the analytical frequency dependent expression for the temperature dependence of the wave packet widths (Eqs (12) and (13)) (QNM/ET, solid line) and in QNMs with the high-temperature approximation (Eq (14)) (QNM/HT, dashed line). The same decoherence function from Cartesian coordinates in the high-temperature limit (CC/HT, dotted line) is also shown for comparison. The inset displays the individual contributions from each trajectory.

Figure 2. Approximations to the semiclassical decoherence function in QNMs with the exact temperature expression (Eqs (13) and (14)) (solid line). The dashed line corresponds to the decorrelated expression (Eq (16)), the dotted line to the overlap approximation (Eq (18)).

Figure 3. Contributions to the decoherence function: $\langle D_x(t)\rangle_T$ (dotted line), $\langle D_p(t)\rangle_T$ (dash-dot line) and the real part of $\langle D_{xp}(t)\rangle_T$ (dash-dot-dot line) (see Eq (19)). The product of these three terms is represented by the dashed line. The full decoherence function (solid line) is also shown for comparison.

Figure 4. Contributions of individual nuclear modes to coordinate and momentum components of the decoherence function (Eq (20)). The top figure shows the displacement terms $\left\langle d_{i,x}(t)\right\rangle_T$, the bottom the momentum change contributions $\left\langle d_{i,p}(t)\right\rangle_T$.

Figure 5. Contributions of individual nuclear modes to coordinate and momentum components of the decoherence function (Eq (20)) at very short times. The top figure shows the displacement terms $\left\langle d_{i,x}(t)\right\rangle_T$, the bottom the momentum change contributions $\left\langle d_{i,p}(t)\right\rangle_T$.

Figure 6. Comparison of the semiclassical decoherence function (solid line) to the lowest-order short-time approximation (Eq (10)) in the high-temperature limit (width, Eq (14)) (dotted line) and with the exact model temperature dependence (width, Eqs (12) and (13)) (dashed line). The t^4-corrected function (Eq (21)) is also shown.

Figure 7. Contributions of individual nuclear modes d_i to the decoherence function in the short-time approximation. The d_i are defined by $D(t) = \exp\left[-\sum_{i(\text{modes})} d_i t^2\right]$ (cf. Eq (10)).

Figure 8. Equilibrium and non-equilibrium solvent response functions ($C(t)$ (Eq (23)) and $S(t)$ (Eq (22)) solid and dashed lines, respectively) following the electronic transition of a solvated electron from the equilibrium excited state to the ground state.

Figure 1.

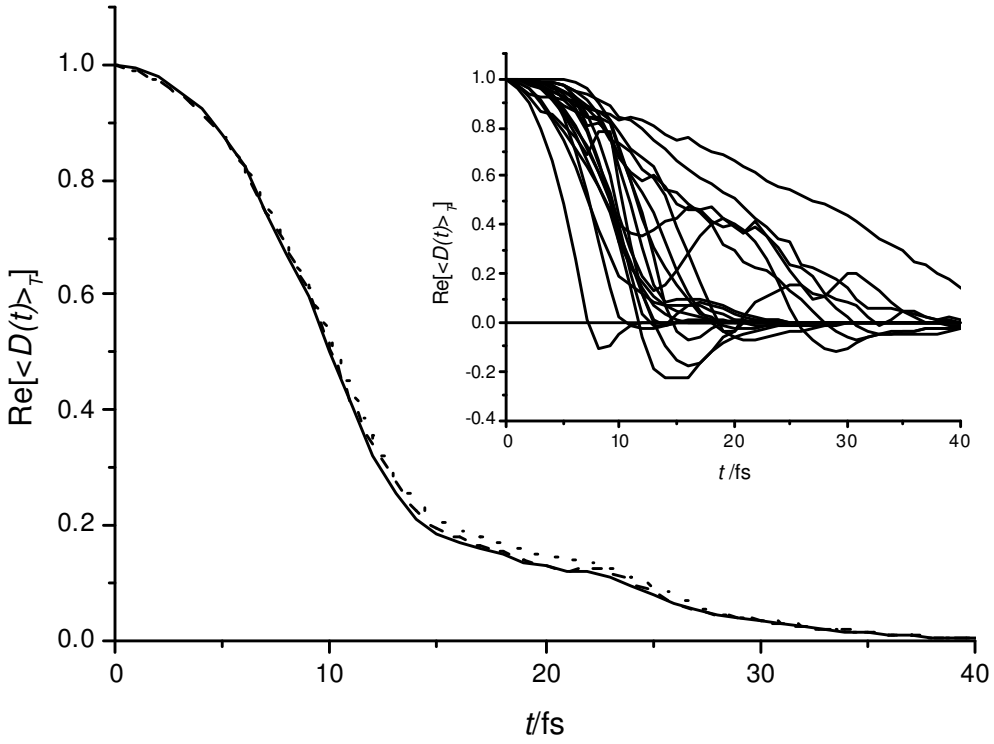
Re[<D(t)>τ]
t/fs
1.0
0.8
0.6
0.4
0.2
0.0
0
10
20
30
40
Re[<D(t)>τ]
t /fs
1.0
0.8
0.6
0.4
0.2
0.0
-0.2
-0.4
0
10
20
30
40

Figure 2.

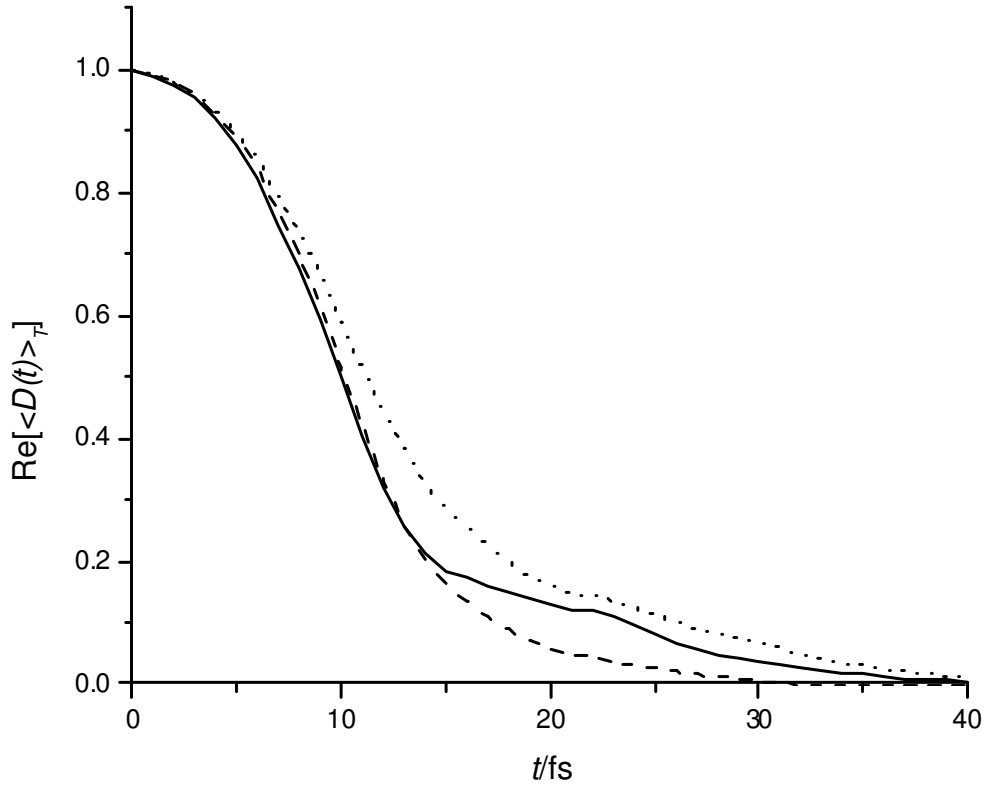

Figure 3.

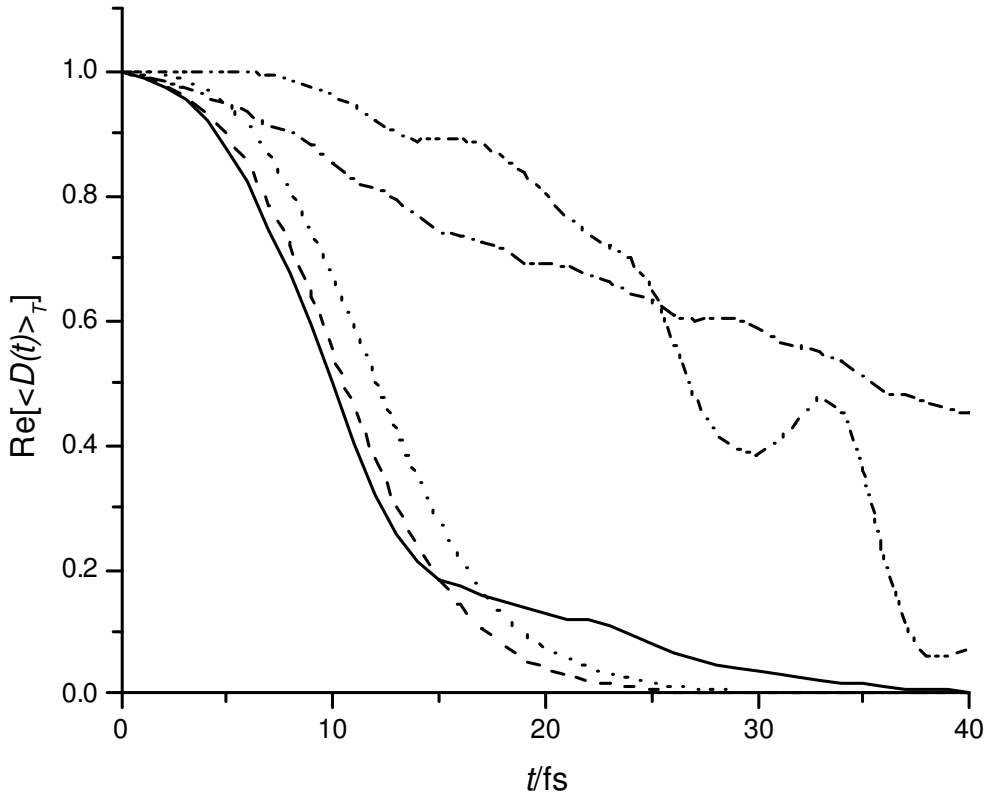

Figure 4.

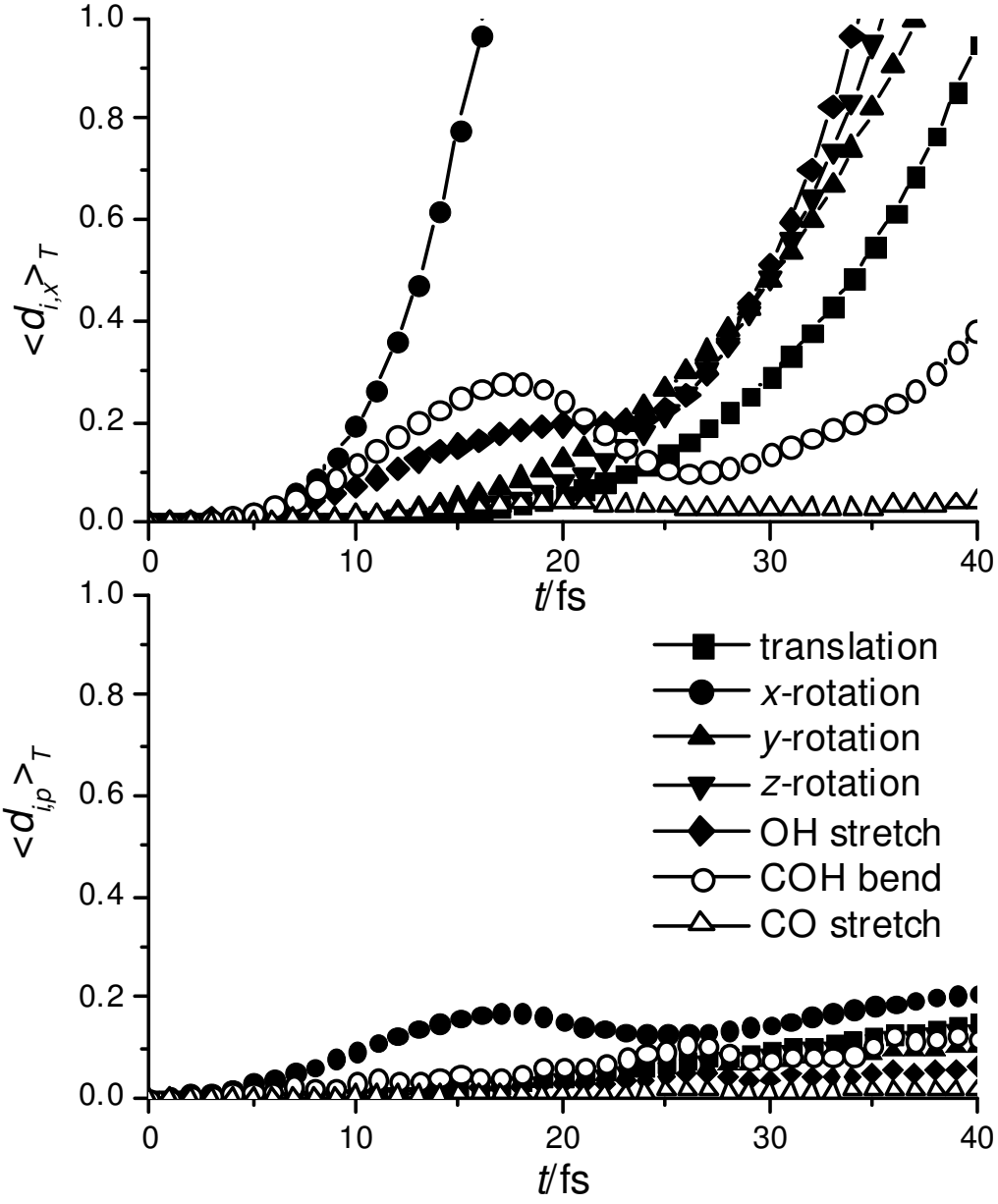
1.0
0.8
0.6
0.4
0.2
0.0
$\langle d_{i,x} \rangle_T$
0
10
20
30
40
t/fs
$\langle d_{i,p} \rangle_T$
translation
x-rotation
y-rotation
z-rotation
OH stretch
COH bend
CO stretch

Figure 5.

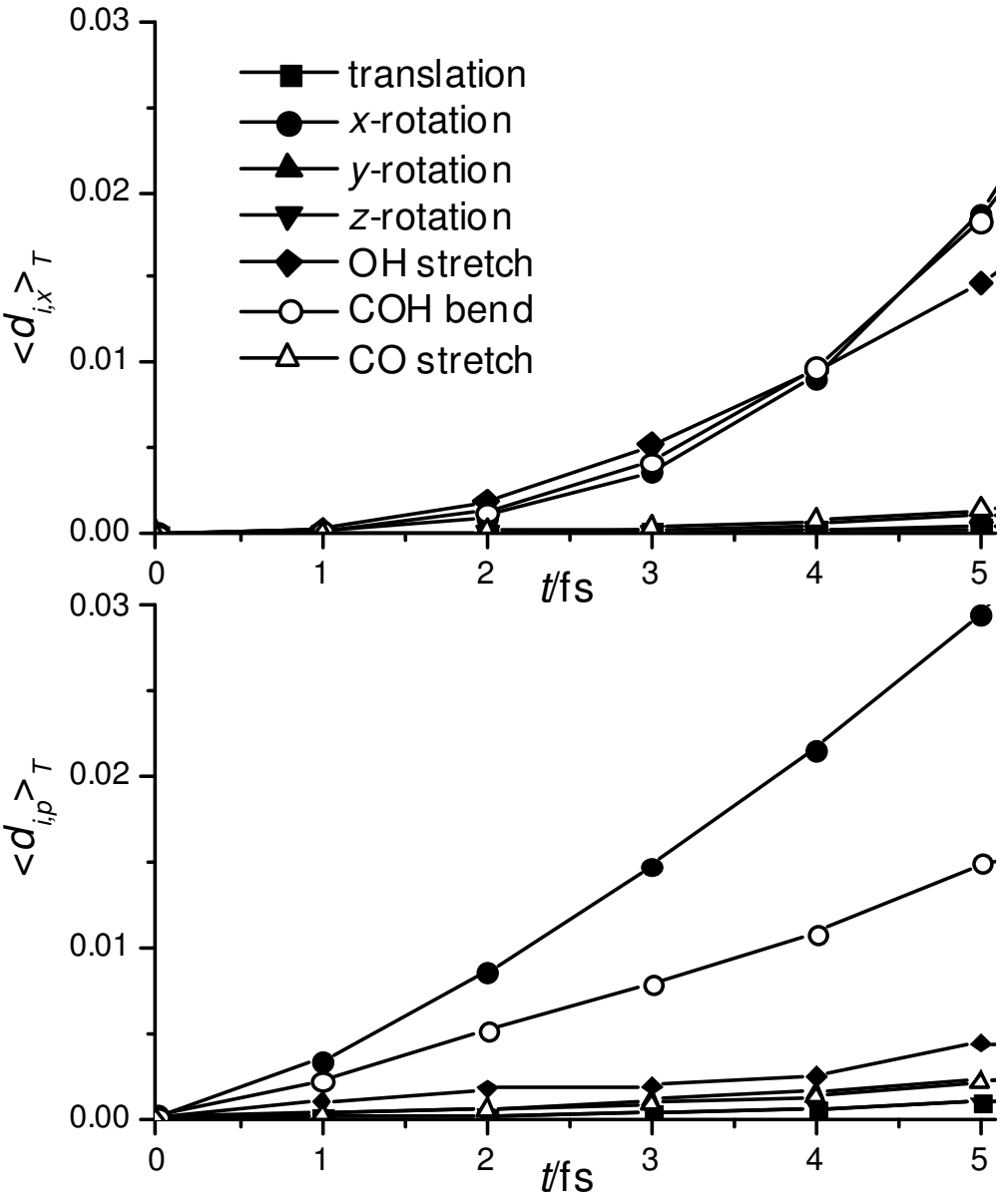
translation
x-rotation
y-rotation
z-rotation
OH stretch
COH bend
CO stretch
<d_{i,x}>_T
<d_{i,p}>_T
t/fs
0.00
0.01
0.02
0.03
0
1
2
3
4
5

Figure 6.

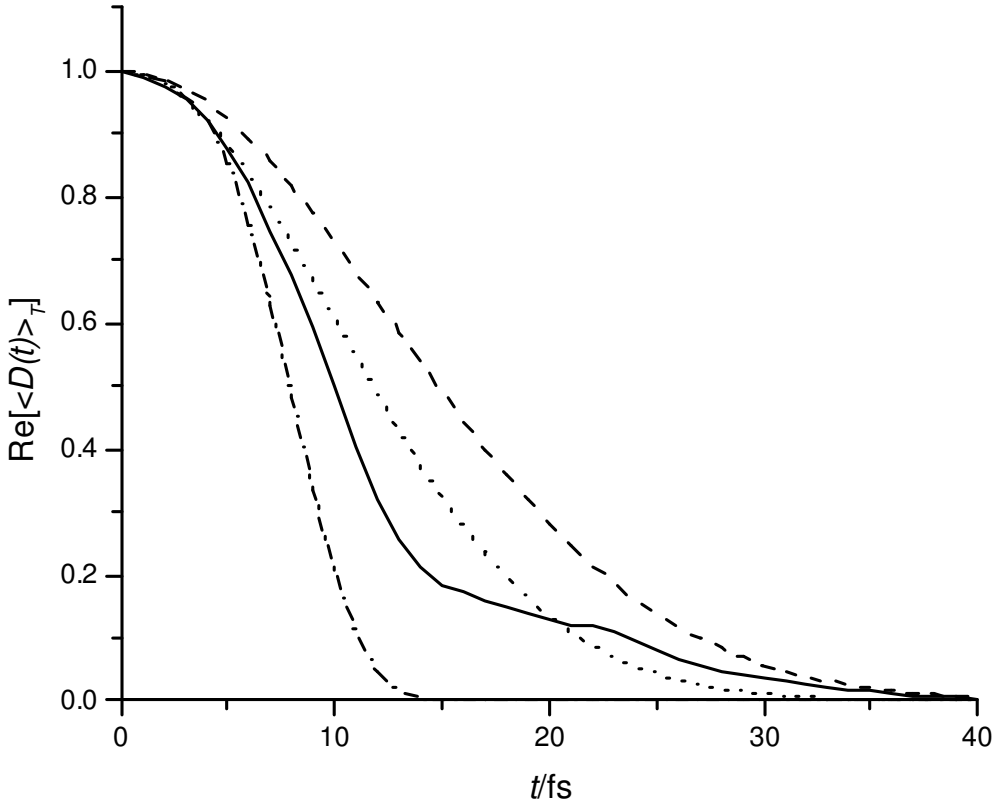

Turi-Rossky

Figure 7.

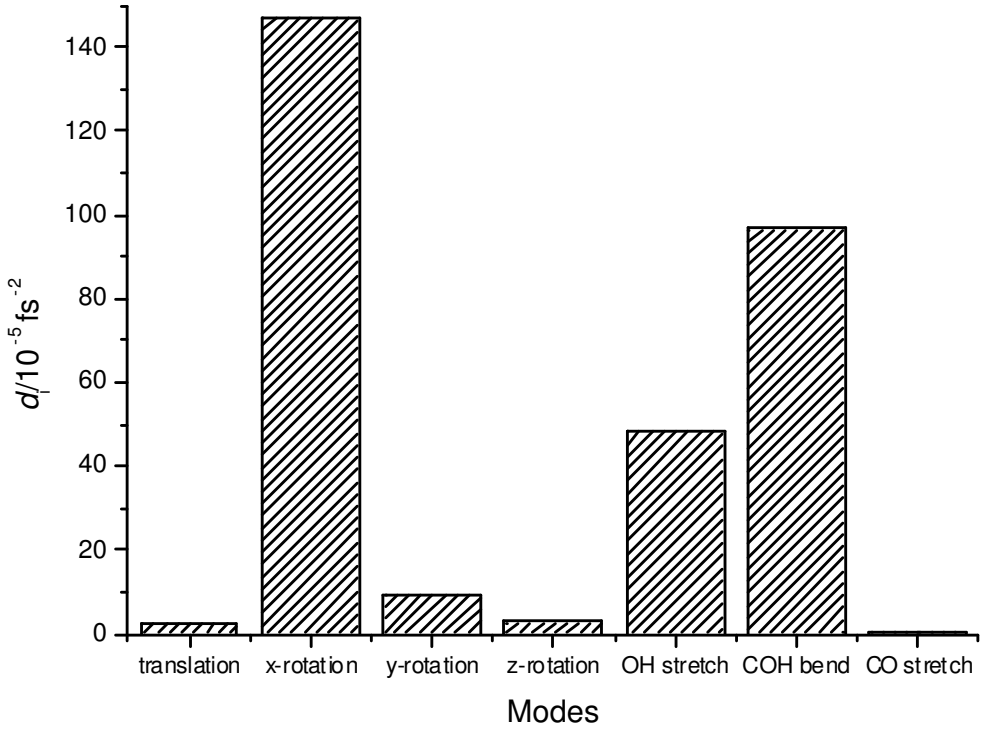

Figure 8.

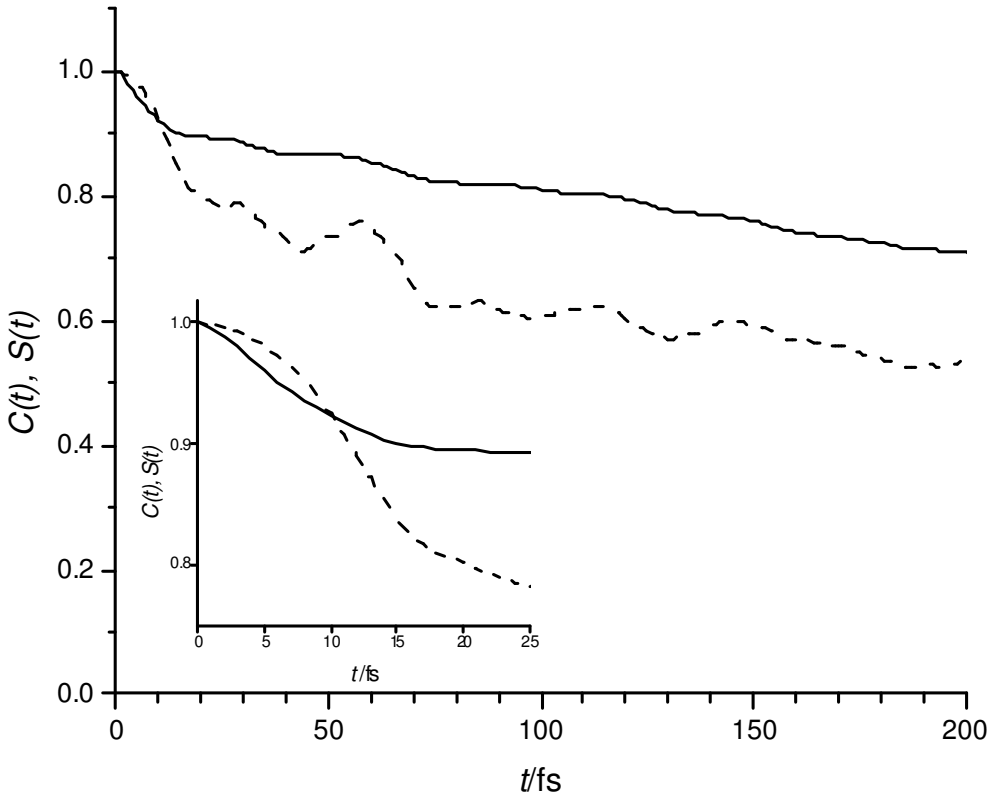
1.0
0.8
0.6
0.4
0.2
0.0
C(t), S(t)
0
50
100
150
200
t/fs
1.0
0.9
0.8
C(t), S(t)
0
5
10
15
20
25
t/fs